Relic Neutrino Background from Cosmic-Ray Reservoirs

Andrea Giovanni De Marchi,* Alessandro Granelli,† Jacopo Nava,‡ and Filippo Sala§
Dipartimento di Fisica e Astronomia, Università di Bologna, via Irnerio 46, 40126, Bologna, Italy; and INFN, Sezione di Bologna, viale Berti Pichat 6/2, 40127, Bologna, Italy

We compute the flux of relic neutrino background (RνB) up-scattered by ultra-high-energy (UHE) cosmic rays (CRs) in clusters that act as CR-reservoirs. The long trapping times of UHECRs make this flux larger than that of RνB up-scattered by UHECRs on their way to Earth, which we also compute. We find that IceCube excludes RνB weighted overdensities larger than 10^{10} in clusters, and that PUEO, RNO-G, GRAND and IceCube-Gen2 will test values down to 10^8. Our treatment incorporates the momentum transfer dependence of the neutrino-nucleus cross section, deep inelastic scattering, a mixed UHECR composition, and flavour information on the up-scattered RνB fluxes for both cases of neutrino mass spectrum with normal and inverted ordering, providing new handles to possibly disentangle the up-scattered RνB from cosmogenic neutrinos.

Introduction— The relic neutrino background (RνB) is referred to as the "Holy Grail" of neutrino physics. It is the only sub-component of dark matter that is predicted by the standard cosmological model (ΛCDM), with a present temperature and number density per-flavour (counting neutrinos and antineutrinos separately) of [1]

$$T_{\nu,0} \simeq 1.67 \times 10^{-4}\,\mathrm{eV}, \quad n_{\nu,0} \simeq 56\,\mathrm{cm}^{-3}. \tag{1}$$

Its detection would give new observational access to the earliest cosmological times ever probed. We have indirect evidence for it via early Universe observations [2, 3], but none of the existing techniques to detect the local RνB is expected to discover it in the foreseeable future, see [4] for a recent overview. It has been furthermore pointed out that PTOLEMY [5], which aims at detecting the RνB by capture on tritium, is insensitive to it because of Heisenberg uncertainty [6, 7]. Experiments aiming at detection of the local RνB then only test the case where its local density is much larger than the diffuse cosmological one $n_{\nu,0}$ by an overdensity factor $\eta_\nu^{\rm Earth} > 1$. The strongest such limit has been set by the KATRIN experiment [8] and reads $\eta_\nu^{\rm Earth} < 1.3 \times 10^{11}$, in the same ballpark of limits from the RνB gravitational effects in the Solar System [9]. Given that gravitational clustering can induce at most $\eta_\nu^{\rm Earth} \sim 10^2$ [10], these experiments then only test the beyond the Standard Model (BSM) scenarios, if any, that lead to those large local overdensities.

The main challenge to detect the RνB is its tiny energy, as a consequence of its low temperature $T_{\nu,0}$. A possible way-out consists in looking for consequences of the highest-energy scatterings that the RνB can undergo in the Universe, so to maximise their SM cross sections. To our knowledge, the first exploration along these lines was the computation of the RνB flux up-scattered by ultra-high-energy (UHE) cosmic rays (CRs), carried out by Hara and Sato in the 80's [11, 12], when much less than today was known about both neutrinos and UHECRs. This idea has been dormant for forty years, until the authors of [13] revived it and, from the non-observation of such an up-scattered RνB flux at IceCube, constrained overdensities in the ballpark of $10^{13}\,(10^{11})$ on scales of about 10 kpc in the Milky Way (around the blazar TXS 0506+056). While the study [13] is sufficient to set a rough limit, it has limitations, like assuming that all UHECRs are protons (which we know is not the case [14, 15]), as well as using an oversimplified SM cross section. These should be addressed in order to possibly hope to detect the up-scattered RνB flux and disentangle it from other neutrinos that could show up in a similar energy range, like cosmogenic ones.[1]

The RνB overdensities tested by the techniques above are not only considerably larger than those achievable via gravitational clustering [10], but also violate the Pauli exclusion principle unless one introduces BSM physics that would cluster the RνB more than gravity, see [23] for a systematic assessment. To our knowledge, the largest overdensities achieved in a fully worked-out BSM model rely on a tiny long-range neutrino self-interaction [24]. They read $\eta_\nu^{\rm BSM} \simeq 10^7\,(m_\nu/0.1~\mathrm{eV})^3$, where m_ν is the neutrino mass scale, and extend up to a volume of the size of a galaxy cluster, motivating to test large overdensities in these environments.

In this letter, we propose to look for the RνB up-scattered by UHECRs in clusters that act as CR-reservoirs [25–31] and calculate the associated fluxes. This idea benefits from the long trapping times of CRs in these environments, and from the knowledge on them that is available today and will increase with upcoming observations in the near future. Additionally, we improve over [13] in the calculation of UHECR-up-scattered RνB fluxes in a number of ways, which we will show to be quantitatively important.

---

[1] The RνB could also be indirectly tested via features that its scatterings induce in UHE neutrinos on their way to Earth [16, 17]. IceCube observations constrain this way $\eta_\nu \lesssim 10^{11}\,(10^8)$ on scales of 10 kpc (of the 14 Mpc that separate us from NGC 1068) [18]. Resonant dips in UHE cosmogenic neutrinos [19], not observed so far [20, 21], could at best test $\eta_\nu \sim 10^{11}$ on scales of the entire Universe [22], which are already ruled-out by not over-closing it.

Up-scattering the RνB with CRs— The flux of accelerated relic neutrinos per unit energy E_ν, from the up-scattering environments of interest, can be written as

$$\frac{d\Phi_\nu}{dE_\nu} = D_{\rm eff}\, n_{\nu,0}\, \bar{\eta}_\nu \int_{E_{\rm CR}^{\rm min}(E_\nu)}^{E_{\rm CR}^{\rm max}} dE_{\rm CR} \frac{d\Phi_{\rm CR}}{dE_{\rm CR}} \frac{d\sigma_{\nu {\rm CR}}}{dE_\nu}, \qquad (2)$$

where the effective distance $D_{\rm eff}$ contains information on the spatial distribution of relic neutrinos and CRs; $\bar{\eta}_\nu \equiv (1/V) \int_V d^3\vec{r}\ \eta_\nu(\vec{r})$ is the RνB overdensity averaged over the volume V, with $\eta_\nu(\vec{r}) = n_\nu(\vec{r})/n_{\nu,0}$ and $n_\nu(\vec{r})$ being the neutrino number density at position $\vec{r}$; $E_{\rm CR}^{\rm min}(E_\nu)$ is the greatest value between the minimal available CR energy and the lowest energy required by the kinematics of the scattering; $E_{\rm CR}^{\rm max}$ is the largest CR energy in their flux; $d\Phi_{\rm CR}/dE_{\rm CR}$ is the CR flux per unit of CR energy $E_{\rm CR}$; $d\sigma_{\nu{\rm CR}}/dE_\nu$ is the differential cross section for the ν-CR scattering. The total neutrino flux is understood to be the sum of Eq. (2) over all neutrinos and nuclear species composing CRs.

Neutrino-nucleus scattering at UHEs— We consider the up-scattering of a relic (anti)neutrino ν ($\bar{\nu}$) by a cosmic nucleus $\mathcal{N}$ via pure SM neutral current (NC) interaction. At the ν-$\mathcal{N}$ exchanged energies that we are interested in, the scattering is described by that on the nucleons $N = p, n$ as

$$\frac{d\sigma_{\nu\mathcal{N}}}{dE_\nu}(E_\mathcal{N}) \simeq \frac{A_\mathcal{N}}{2}\left[\frac{d\sigma_{\nu p}}{dE_\nu}\left(\frac{E_\mathcal{N}}{A_\mathcal{N}}\right) + \frac{d\sigma_{\nu n}}{dE_\nu}\left(\frac{E_\mathcal{N}}{A_\mathcal{N}}\right)\right], \qquad (3)$$

where we have focused for simplicity on isoscalar nuclei with equal number $A_\mathcal{N}/2$ of protons and neutrons, each carrying a fraction $1/A_\mathcal{N}$ of the nucleus's energy $E_\mathcal{N}$, and summed over elastic scattering (ES) and deep inelastic scattering (DIS) contributions: $d\sigma_{\nu N}/dE_\nu = d\sigma^{\rm ES}_{\nu N}/dE_\nu + d\sigma^{\rm DIS}_{\nu N}/dE_\nu$. The ES part, summed over ν and $\bar{\nu}$, reads [32, 33]

$$\frac{d\sigma^{\rm ES}_{\nu N}}{dE_\nu} = \frac{2G_F^2 m_\nu m_N^4}{\pi(s-m_N^2)^2}\left[A_N(Q^2) + C_N(Q^2)\frac{(s-u)^2}{m_N^4}\right], \qquad (4)$$

where G_F is the Fermi constant; $s = 2m_\nu E_N + m_N^2 + m_\nu^2$, $Q^2 = 2m_\nu(E_\nu - m_\nu)$ is the momentum transfer squared, $u = 2m_\nu^2 + 2m_N^2 - s + Q^2$; $m_{N(\nu)}$ is the nucleon (neutrino) mass and $E_{N(\nu)}$ is the energy of the incoming nucleon (outgoing neutrino) in the frame in which the initial neutrino is at rest. The functions A_N and C_N are given in Appendix A (see, e.g., [32, 33]) and strongly suppress ES for $Q^2 \gtrsim m_N^2 \approx \mathrm{GeV}^2$. The DIS, in which the initial neutrino interacts directly with the quark constituents of the nucleons, takes over for $E_N \gtrsim 10^{10-11}$ GeV, given $Q^2 \lesssim s$ and $m_\nu \approx 0.1\,$eV, thus being necessary to describe the highest-energy part of the up-scattered RνB flux. For the NC ν-N DIS cross section we adopt

$$\frac{d\sigma^{\rm DIS}_{\nu N}}{dE_\nu} \simeq \sum_{a=q,\bar{q}} \frac{G_F^2[(g_V^a)^2 + (g_A^a)^2]}{2\pi E_N} \times \int_{y_{\rm min}}^1 \frac{dy}{y^2}\frac{Q^2 f_a^N(x,Q^2)}{[1+Q^2/M_Z^2]^2}\left(y^2 - 2y + 2 - \frac{2m_N^2}{Q^2}\right), \qquad (5)$$

where M_Z is the Z boson mass, y is the inelasticity parameter satisfying $y_{\rm min} = (E_\nu - m_\nu)/E_N \lesssim y \le 1$, $x = (E_\nu - m_\nu)/(E_N y)$ is the Bjorken scaling variable and $f_a^N(x, Q^2)$ is the parton distribution function (PDF) for the quark a having NC vector and axial coupling g_V^a and g_A^a, $a = u, d, s, c, b$ (we neglect any contribution from the top quark). We evaluate the PDFs with the Python package `parton` using the "CT10" PDF set [34] (see also this website for more details). Details on the derivation of Eq. (5) are given in Appendix B. For simplicity, we do not take the coherent ν-$\mathcal{N}$ scattering into account as it could contribute only at energy scales smaller than those of interest to our study [33, 35], and neglect the contribution to $d\sigma_{\nu\mathcal{N}}/dE_\nu$ from hadronic resonances [36, 37], relevant for $Q^2 \approx \mathrm{GeV}^2$, so that in the considered range our results are conservative.

CRs up-scattering RνB en route to Earth— As they travel towards the Earth, UHECRs up-scatter the RνB with the largest cross sections among all CRs, and induce a flux described by Eq. (2). While the bulk of CRs with energy much below the EeV are believed to originate within the Milky Way (MW) [38, 39] and to be mostly protons below the PeV [40], UHECRs above the EeV scale are today understood as having an extragalactic origin, see e.g. [41–43], and a mixed composition with heavier nuclei dominating over protons, see e.g. [14, 15, 44–49]. We therefore employ the CR spectrum $d\Phi_{\rm CR}/dE_{\rm CR}$ from [14] and, by considering up-scatterings in the MW with $D_{\rm eff} \approx 10$ kpc (see e.g. [50–52]), we obtain the flux reported as a dot-dashed line in Fig. 1 (see further). Our calculation improves over the analogous one [13] by going beyond the proton-only composition of CRs and by implementing the momentum transfer dependence and DIS in the cross section. It results in a significantly different flux with respect to [13], see Appendix C for details of the comparison.

Since tentative sources of UHECRs are located at $1 \sim 100\,$Mpc from Earth [53–57], $D_{\rm eff}$ can be larger than 10 kpc by orders of magnitude, resulting in a sensitivity to $\bar{\eta}_\nu \sim 10^{10-11}$. Still, these enormous $\bar{\eta}_\nu$ over such long distances are hard to justify without spoiling the large-scale homogeneity of the Universe, motivating us to look for environments where $D_{\rm eff}$ can be sizeable while keeping neutrino overdensities localised on smaller scales.

Boosted RνB from CR-reservoirs— A possible explanation for the extragalactic origin of UHECRs is that they are produced inside galaxy clusters, in which they reside up to cosmological times before escaping and contributing to the UHECR flux on Earth [25–31] (see also [58] for a review). The distance they travel inside these gigantic CR-reservoirs would be roughly $c\tau_{\rm esc} \simeq 0.3\,{\rm Gpc}\,(\tau_{\rm esc}/1\,{\rm Gyr})$, where $\tau_{\rm esc}$ is the time CRs spend in the cluster before their release. The effective distance entering Eq. (2) can be written as $D_{\rm eff} = \mathcal{B} c\tau_{\rm esc}$, having defined the spatial boost factor

$$\mathcal{B} \equiv \int_V d^3\vec{r} f_{\rm CR}(x)\,\delta_\nu(\vec{r})\,, \tag{6}$$

with $\delta_\nu(\vec{r}) \equiv \eta_\nu(\vec{r})/\bar{\eta}_\nu$ and $f_{\rm CR}(\vec{r})$ the spatial profile of the CR flux inside a CR-reservoir of volume V, normalised such that $\int_V d^3\vec{r} f_{\rm CR}(\vec{r}) = 1$. One has $\mathcal{B} = 1$ for a homogeneous RνB, $\delta_\nu(\vec{r}) = 1$, while $\mathcal{B} > 1$ if, e.g., the number densities of both UHECRs and neutrinos are peaked at small radii. In what follows, we fix $\mathcal{B} = 1$ and $\tau_{\rm esc} \simeq 2\,{\rm Gyr}$ [30], neglecting any dependence on the CR energy that $\tau_{\rm esc}$ (and $\mathcal{B}$) may have. We checked that implementing the $\tau_{\rm esc}$ energy-dependence, as derived in, e.g., [31], does not significantly alter our results.

We model UHECRs in cluster reservoirs following [30]. For each nucleus $\mathcal{N}$, we write

$$\frac{d\Phi_{\mathcal{N}}}{dE_{\mathcal{N}}} = K_{\mathcal{N}} \left(\frac{E^{\rm max}_{\mathcal{N}}}{E_{\mathcal{N}}}\right)^{\alpha} e^{-E_{\mathcal{N}}/E^{\rm max}_{\mathcal{N}}}\,, \tag{7}$$

where $2 \leq \alpha \leq 2.5$ and $E^{\rm max}_{\mathcal{N}}/Z_{\mathcal{N}} \simeq 7.69 \times 10^{10}{\rm GeV}$, $Z_{\mathcal{N}}$ being the atomic number of $\mathcal{N}$. We consider the relative nuclear abundances as given in [30] and fix the normalisation factors $K_{\mathcal{N}}$ by requiring that the total luminosity emitted from the entire population of CR-reservoirs matches with the one observed at Earth. Concentrating on the energy range $E^{\rm ankle}_{\rm CR} = 5$ EeV $\leq E_{\rm CR} \leq 200\,{\rm EeV}$, approximating the observed extragalactic CR spectrum as a single power-law $d\Phi_{\rm CR}/dE_{\rm CR} \simeq (d\Phi_{\rm CR}/dE_{\rm CR})_{\rm ankle}\,(E^{\rm ankle}_{\rm CR}/E_{\rm CR})^{2.5}$, with $(d\Phi/dE_{\rm CR})_{\rm ankle} \simeq 10^{-27}\,{\rm GeV^{-1}cm^{-2}s^{-1}sr^{-1}}$ [14], and taking as a benchmark value $\alpha = 2.3$ [30], we find $K_{\rm H(He)} \simeq 9.44\times10^{-31}\,(9.52\times10^{-32})\,{\rm GeV^{-1}cm^{-2}s^{-1}sr^{-1}}$ for ^{1}H (^{4}He), while heavier nuclei are sub-dominant. We give more details on the normalisation procedure in Appendix D.

The resulting total flux on Earth of relic neutrinos up-scattered in CR-reservoirs is shown in Fig. 1. We compare it with current observations, limits and future sensitivities, and with the flux of cosmogenic neutrinos arising as secondary products of UHECRs interactions inside reservoirs as computed in [30], because that could constitute a background to our signal. The total flux is obtained by summing over all neutrino mass eigenstates ν_i having non-zero masses m_i, $i = 1, 2, 3$, squared mass differences $\Delta m^2_{21} \equiv m_2^2 - m_1^2 = 7.42 \times 10^{-5}\,{\rm eV}^2$ and $\Delta m^2_{31} \equiv m_3^2 - m_1^2 = 2.507 \times 10^{-3}\,{\rm eV}^2$ [72], sum of neutrino masses saturating the cosmological limit $\sum_i m_i = 0.113\,{\rm eV}$ [59] for a spectrum with normal ordering (NO) $m_1 < m_2 < m_3$ and a weighted overdensity of $\mathcal{B}\bar{\eta}_\nu = 3 \times 10^8$.

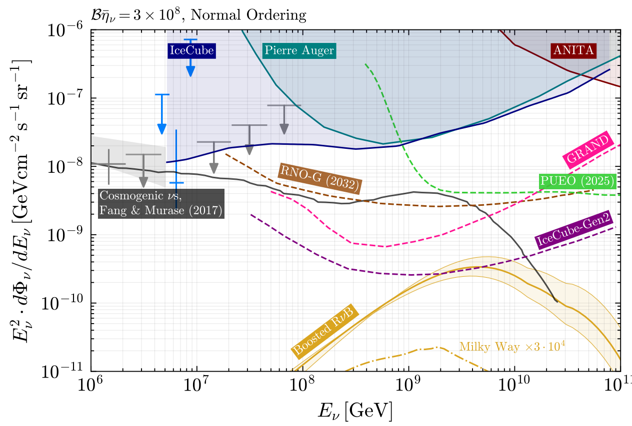

FIG. 1. The all-flavour RνB fluxes on Earth as up-scattered by UHECRs inside galaxy clusters acting as CR-reservoirs (continuous gold lines) or from UHECRs in the MW travelling towards Earth (dot-dashed gold line, multiplied by 3×10^4 to show in the plot). The yellow shaded region is obtained by varying the slope of the CR spectrum in reservoirs within $2 \leq \alpha \leq 2.5$ (central thick line, $\alpha = 2.3$), for a weighted RνB overdensity $\mathcal{B}\bar{\eta}_\nu = 3 \times 10^8$, a neutrino mass spectrum with NO and $\sum_i m_i = 0.113\,{\rm eV}$ [59]. We depict in grey the 95% C.L. band of the single-power-law model for the astrophysical muon neutrino-induced tracks detected at IceCube [60]. The crosses (arrows) are piece-wise best-fit $\pm1\sigma$ events (68% C.L. limits) for cascades and showers initiated by astrophysical neutrinos at IceCube [61, 62] (see also [63, 64], the KM3NeT ARCA detector will have a similar sensitivity [65]). Fluxes of UHE neutrinos lying in the upper shaded regions are excluded at 90% C.L. by the null-detection at IceCube [20], Pierre Auger Observatory [21] and ANITA [66]. Sensitivities of PUEO (2025) [67], RNO-G (2032, first stations already taking data) [68], IceCube-Gen2 [69] (planned) and GRAND [70] (proposed) are depicted as dashed lines. The black line displays the cosmogenic neutrino flux from [30].

Limits and sensitivities on RνB overdensities— In Fig. 2 we show the limits and sensitivities on the combination of parameters $\mathcal{B}\bar{\eta}_\nu$, as a function of the lightest neutrino mass assuming NO. We derive them by imposing that our flux line touches the relevant limit/sensitivity curve. Results for inverted ordering (IO) $m_3 < m_1 < m_2$ are similar and shown in Appendix E.

Our limits and sensitivities are compared with the Pauli exclusion principle constraining the number density of gravitationally-bound neutrinos, when no BSM clustering effect is assumed. We compute the local maximum overdensity as prescribed in [10] for a galaxy cluster of mass $M = 5\times10^{15} M_\odot$, assuming a Navarro-Frenk-White (NFW) [73] profile for the surrounding dark matter halo, and then average over the cluster volume.

We also evaluate the overdensity $\bar{\eta}_\nu$ for which the RνB mass equals that of the entire galaxy cluster. We consider a NFW dark matter density profile whose virial radius scales as $R_{\rm vir} \sim M^{1/3}$, such that the average mass density in clusters $\rho_{\rm cluster}$ is independent of the cluster mass. In particular, $\rho_{\rm cluster} \approx 200\rho_c$ [74], with $\rho_c \simeq 1.05\times10^{-5}h^{-2}\,{\rm GeV\,cm^{-3}}$ the critical density of the Universe and $h \simeq 0.674$ the dimensionless Hubble parameter. We then impose a rough cluster mass limit by requiring $\bar{\eta}_\nu n_{\nu,0}\sum_i m_i \leq \rho_{\rm cluster}$, taking equal averaged overdensity for each neutrino species. The corresponding limit on the weighted overdensity $\mathcal{B}\bar{\eta}_\nu$ can be relaxed for non-uniform neutrino and CR spatial distributions.

Finally, we estimate the sensitivity of the proposed PTOLEMY experiment [7] on local neutrino overdensities, considering the configuration where the final $^3{\rm He}^+$ is in the bound ground state. Depending on the neutrino mass compared to the experimental resolution Δ (we use $\Delta = 0.05$ eV as reference), the RνB absorption peak can be well-separated from the continuous β-decay spectrum or hidden under it. Accordingly, we require at least $N_{\rm peak} = 10$ events/yr to call a detection in the first situation, or $N_{\rm peak} \gtrsim 3\sqrt{N_{\rm bkg}}$, with $N_{\rm bkg}$ the number of β-decay events/yr in the same energy range in the second.

Flavour composition of the boosted RνB— Neutrinos produced in astrophysical environments typically exhibit precise flavour composition at the source, but neutrino oscillations over astronomical distances tend to homogenise any flavour disparity [76, 77].

Instead, the boosted RνB exhibits a peculiar flavour composition. At first, the RνB is evenly distributed among the mass eigenstates, which directly take part in the NC scatterings with UHECRs. The mass eigenstates ν_i then propagate freely and their fluxes $d\Phi_i/dE_\nu$ are preserved. At detection, the probability of observing a massive neutrino ν_i in a flavour $\ell = e, \mu, \tau$ is $\mathcal{P}_{\ell i} = |U_{\ell i}|^2$, with $U_{\ell i}$ being the entries of the Pontecorvo-Maki-Nakagawa-Sakata (PMNS) neutrino mixing matrix [78–80]. Then, the flux of boosted neutrinos with flavour ℓ is given by $d\Phi_\ell/dE_\nu = \sum_i |U_{\ell i}|^2\, d\Phi_i/dE_\nu$. Clearly, the relative flux in each flavour depends on the neutrino mixing parameters through the PMNS matrix and neutrino masses via the differential flux.

As the fluxes of the different mass eigenstates have distinct energy dependence, the flavour composition of the boosted RνB flux depends on the energy as well. It is nevertheless practical to calculate an integrated flavour ratio $\Phi_\ell/\Phi_{\rm tot} \equiv \sum_i |U_{\ell i}|^2\Phi_i/\sum_i\Phi_i$. The predicted integrated flavour composition is shown in Fig. 3. In the plot, the parameters of the PMNS matrix are varied within the 3σ ranges allowed by the `NuFit 5.2` global analysis of neutrino oscillation data [71, 72], while $m_{1(3)}$ in the range $10^{-3} \leq m_{1(3)}/{\rm eV} \leq 1$, for NO (IO). As $m_{1(3)}$ increases, the mass eigenstates become nearly degenerate, implying $\Phi_1 \simeq \Phi_2 \simeq \Phi_3$ and an unflavoured composition $\Phi_e : \Phi_\mu : \Phi_\tau = 1 : 1 : 1$, due to the unitarity

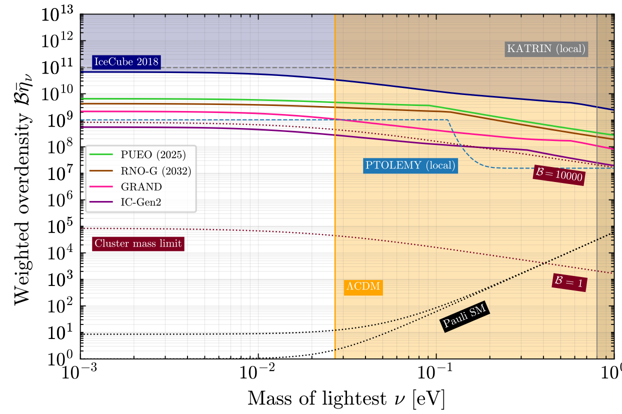

FIG. 2. RνB overdensity $\bar{\eta}_\nu$ spatially averaged on galaxy clusters and weighted by the spatial boost factor $\mathcal{B}$ of Eq. (6), versus the lightest neutrino mass. Assuming the reference slope $\alpha = 2.3$ in the CR spectrum in CR-reservoirs, and a neutrino mass spectrum with NO, we derive the 90% C.L. constraint set by the null-detection at IceCube [20] (blue shaded) and the sensitivities at PUEO (2025) [67], RNO-G (2032) [68], GRAND [70] and IceCube-Gen2 [69] (solid lines, top to bottom). We also display the KATRIN limit $m_\nu < 0.8$ eV at 90% C.L. [75], holding for both Dirac and Majorana neutrinos (gray shaded), and the DESI one assuming ΛCDM [59] $\sum_i m_i < 0.113$ eV at 95% C.L. (orange shaded). We also derived the maximum $\bar{\eta}_\nu$ in a galaxy cluster allowed by i) the Pauli exclusion principle in the SM and for a galaxy cluster of reference mass $5\times10^{15}M_\odot$ [10] (black dotted), respectively for the heaviest (upper line) and lightest (lower line) neutrino, displayed for $\mathcal{B} = 1$; ii) requiring that the RνB does not overshoot the mass of the host galaxy cluster (red dotted), displayed for $\mathcal{B} = 1$ (upper), 10^4 (lower). Despite holding for overdensities on Earth and not in galaxy clusters, we also display the KATRIN limit $\eta_\nu^{\rm Earth} < 9.7\times10^{10}$ [8] (dashed gray) and the PTOLEMY sensitivity on $\eta_\nu^{\rm Earth}$ that we derived from [7] (dashed cyan).

of the PMNS matrix. By decreasing $m_{1(3)}$, the mass spectrum becomes hierarchical with $m_1 \lesssim m_2 \ll m_3$ ($m_3 \ll m_1 \lesssim m_2$) with the (two) heaviest neutrino(s) dominating the total flux. In this situation, because of the structure of the PMNS matrix, the flavour flux composition is approximately $0:1:1$ $(2:1:1)$ for NO (IO). This could help UHE neutrino observatories discriminate between a boosted RνB signal and other kinds of astrophysical neutrino fluxes [67, 70, 81–84].

Conclusions— We computed the flux of relic neutrinos up-scattered by UHECRs via SM NC interactions, taking into account the full Q^2-dependence and DIS in the cross section, and the mixed CR composition. Our results are shown in Fig. 1 for up-scatterings in the MW by UHECRs travelling towards Earth and in galaxy clusters acting as CR-reservoirs. These objects constitute an ideal environment because of the long trapping times of CRs inside them, and indeed lead to the largest RνB

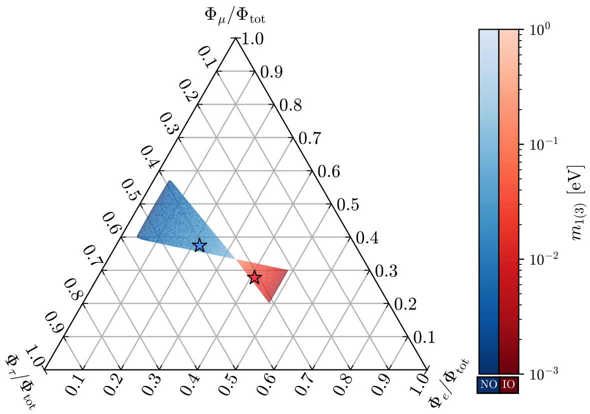

FIG. 3. Flavour composition of the boosted RνB. The blue (red) area is obtained by varying the PMNS matrix entries and squared neutrino mass splittings within the 3σ allowed range [72], assuming a neutrino mass spectrum with NO (IO). Darker regions correspond to lighter $m_{1(3)}$. The stars mark the flavour composition of the boosted RνB for the best-fit values of the neutrino oscillation data and $m_{1(3)}$ saturating the cosmological bounds $\sum_i m_i = 0.113\,(0.145)\,\mathrm{eV}$ [59] (the flavour composition depends only very slightly on the slope of the CR spectrum).

up-scattered fluxes. Our calculation is conservative, having not included the hadron-resonances contributions to ν-UHECR scatterings, nor the secondary neutrinos produced by their SM charged-current interactions.

We find that IceCube [20] excludes $\mathcal{B}\bar{\eta}_\nu \gtrsim 10^{10}$ in galaxy clusters, where we weighted the average overdensity $\bar{\eta}_\nu$ by a spatial boost factor $\mathcal{B}$, and that future telescopes [67–70] could possibly detect the boosted RνB for $\mathcal{B}\bar{\eta}_\nu \gtrsim 10^8$, see Fig. 2. These large overdensities require a BSM origin, as could be obtained on the scales of galaxy clusters via, e.g., long-range interactions.

To distinguish a boosted RνB signal from other UHEν fluxes, such as cosmogenic neutrinos, we propose to rely on i) the shape of the energy spectrum, DIS being crucial in determining the one of the up-scattered RνB, and ii) the flavour composition, the specific one of the up-scattered RνB being displayed in Fig. 3.

Our study motivates further UHEν searches at telescopes, a direct implementation of RνB-UHECR scatterings in the modelling of CR-reservoirs and sources, and research on how to obtain the sizeable neutrino overdensities required for a potential detection.

Acknowledgements— We thank Angelo Esposito for precious elucidations on the PTOLEMY experimental set-up and Silvia Pascoli for useful discussions. We acknowledge the use of computational resources from the parallel computing cluster of the Open Physics Hub (https://site.unibo.it/openphysicshub/en) at the Physics and Astronomy Department in Bologna. This work was supported in part by the European Union's Horizon research and innovation programme under the Marie Skłodowska-Curie grant agreements No. 860881-HIDDeN and No. 101086085-ASYMMETRY, by COST (European Cooperation in Science and Technology) via the COST Action COSMIC WISPers CA21106, and by the Italian INFN program on Theoretical Astroparticle Physics.

APPENDICES

Appendix A: Form Factors of the ν-N Neutral Current Elastic Scattering Cross Section

A detailed derivation of the ν-N elastic scattering cross section can be found in, e.g., [32] (see also [33]). Here, for completeness, we only report the form of the factors A_N and C_N appearing in Eq. (4) of the main text in terms of the momentum transfer Q^2. These are given in terms of the weak neutral current form factors by [32, 33]

$$A_N(Q^2) = \frac{Q^2}{m_N^2}\Bigg\{\left(1+\frac{Q^2}{4m_N^2}\right)\left(G_{\rm A}^{ZN}(Q^2)\right)^2 - \left(1-\frac{Q^2}{4m_N^2}\right)\Bigg[\left(F_1^{ZN}(Q^2)\right)^2 + \frac{Q^2}{4m_N^2}\left(F_2^{ZN}(Q^2)\right)^2\Bigg]\Bigg\} \tag{A1}$$

$$C_N(Q^2) = \frac{1}{4}\Bigg[\left(G_{\rm A}^{ZN}(Q^2)\right)^2 + \left(F_1^{ZN}(Q^2)\right)^2 + \frac{Q^2}{4m_N^2}\left(F_2^{ZN}(Q^2)\right)^2\Bigg] \tag{A2}$$

where $F_{1,2}^{ZN}(Q^2) \simeq \pm(1/2)[F_{1,2}^p(Q^2) - F_{1,2}^n(Q^2)] - 2s_{\rm W}^2 F_{1,2}^N(Q^2)$, with F_1^N and F_2^N being respectively the Dirac and Pauli electromagnetic form factors for the nucleon $N = n, p$, with the $+(-)$ sign for $p\,(n)$, $s_{\rm W}^2 \simeq 0.229$ [74] the sine squared of the Weinberg angle, $G_{\rm A}^{Zp}(Q^2) \simeq (1/2)G_{\rm A}(Q^2)$ and $G_{\rm A}^{Zn}(Q^2) \simeq -(1/2)G_{\rm A}(Q^2)$ and $G_{\rm A}(Q^2)$ the axial weak charged current form factor. We have neglected the contributions from the form factors related to strange and heavier quarks, as well as the pseudo-scalar contribution (which vanishes exactly in the case of massless neutrinos). It is useful to define also the electric and magnetic form factors respectively as [85–87]

$$G_{\rm E}^N(Q^2) \equiv F_1^N(Q^2) - \frac{Q^2}{4m_N^2}F_2^N(Q^2), \tag{A3}$$

$$G_{\rm M}^N(Q^2) \equiv F_1^N(Q^2) + F_2^N(Q^2). \tag{A4}$$

At zero momentum transfer, i.e. $Q^2 = 0$, we have $G_{\rm E}^p(0) = 1$, $G_{\rm E}^n(0) = 0$, $G_{\rm M}^p(0) = \mu_p/\mu_N$ and $G_{\rm M}^n(0) = \mu_n/\mu_N$, where μ_N is the nuclear magneton, while $\mu_p \simeq 2.79\mu_N$ and $\mu_n \simeq -1.91\mu_N$ are respectively the magnetic moments of the proton and of the neutron [74]. The

Q^2-dependence of the electric, magnetic and axial form factors is often fitted experimentally against dipole expressions, namely $G_{\rm E,M}(Q^2) = G_{\rm E,M}(0)(1+Q^2/\Lambda^2_{\rm E,M})^{-2}$ with $\Lambda_{\rm E,M} \simeq 0.8\,$GeV, given in terms of the experimentally measured electric charge and magnetic radii of the proton $\langle r^2_{\rm E,M}\rangle^{1/2} = \sqrt{12}/\Lambda_{\rm E,M} \simeq 0.85\,$fm [88, 89], while $G_{\rm A}(Q^2) = G_{\rm A}(0)(1+Q^2/m^2_{\rm A})^{-2}$ with $G_{\rm A}(0) \simeq 1.245$ and $m_{\rm A} \simeq 1.17\,$GeV, from measurements of the axial radius $\langle r^2_{\rm A}\rangle^{1/2} = \sqrt{12}/m_{\rm A} \simeq 0.582\,$fm [90].

Appendix B: Neutral Current Deep Inelastic Scattering Cross Section

If the centre-of-mass energy is sufficiently large, the interaction between a neutrino and a nucleon $N = p, n$ takes place with its constituents through DIS. In this section, we derive the NC DIS cross section assuming a parton model with quarks carrying a fraction ξ of the nucleon's momentum, and then average the results over the quark PDFs. The process is diagrammatically represented below using the Ti*k*Z-Feynamn package [91].

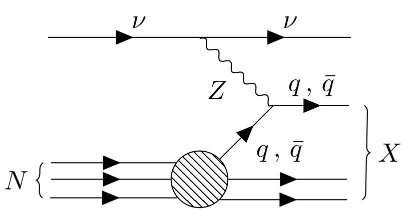

We fix the momenta of the incoming neutrino and quark respectively as $p_\nu = (E_\nu, \vec{p}_\nu)$ and $p_q = (E_q, \vec{p}_q)$. Analogously, for the outgoing neutrino and quarks we define $k_\nu = (E'_\nu, \vec{k}_\nu)$ and $k_q = (E'_q, \vec{k}_q)$, respectively. Furthermore, we neglect the quark masses. The DIS is typically studied in the frame of reference in which the nucleon is at rest $\vec{p}_N = 0$ (LAB), see, e.g., the comprehensive derivation in [32] and references therein (see also [92]). However, we are interested in the frame in which the relic neutrino is at rest instead. Our approach will be that of recovering the DIS cross section in the LAB frame and write it in terms of Lorentz invariants, so to render any change of reference frame immediate. It will prove useful to define also the initial nucleon momentum $p_N = p_q/\xi = (E_N, \vec{p}_N)$ and the 4-momentum transfer $q = p_\nu - k_\nu$. Keeping the same notation as in the main text, we denote the squared centre-of-mass energy and momentum transfer respectively as $s = (p_N + p_\nu)^2$ and $Q^2 = -q^2$. We also define the following Lorentz invariant quantities:

- *energy transfer*

$$\epsilon \equiv \frac{p_N \cdot q}{m_N}; \tag{B1}$$

- *inelasticity*

$$y \equiv \frac{p_N \cdot q}{p_N \cdot p_\nu} = \frac{2\epsilon m_N}{s - m_N^2 - m_\nu^2}; \tag{B2}$$

- *Bjorken scaling variable*

$$x \equiv \frac{Q^2}{2 p_N \cdot q} = \frac{Q^2}{(s - m_N^2 - m_\nu^2)\, y}. \tag{B3}$$

Moreover, we have the following set of relations:

$$Q^2 \overset{\rm LAB}{=} -2m_\nu^2 + 2E_\nu E'_\nu - 2|\vec{p}_\nu||\vec{k}_\nu|\cos\theta, \tag{B4}$$

$$E_\nu \overset{\rm LAB}{=} \frac{s - m_N^2 - m_\nu^2}{2m_N}, \tag{B5}$$

$$E'_\nu \overset{\rm LAB}{=} E_\nu(1-y), \tag{B6}$$

$$v_{\rm rel} \overset{\rm LAB}{=} |\vec{p}_\nu| m_N/(E_\nu E_N), \tag{B7}$$

where θ is the scattering angle in the LAB frame and $v_{\rm rel}$ is the relative velocity between the neutrino and the nucleon. In particular, we have $\partial\cos\theta/\partial x = -m_N E_\nu y/(|\vec{p}_\nu||\vec{k}_\nu|)$ and $\partial E'_\nu/\partial y \overset{\rm LAB}{=} -E_\nu$, so that:

$$\frac{4\pi}{4E_\nu E_N v_{\rm rel}} \frac{d^3 k_\nu}{(2\pi)^3 2E'_\nu} = \frac{y}{8\pi}\left[1 + \mathcal{O}\left(\frac{m_\nu m_N}{p_\nu \cdot p_N}\right)\right] dx dy. \tag{B8}$$

The master formula for the DIS differential cross section can be written as [92]:

$$\begin{aligned} d\sigma^{\rm DIS}_{\nu N} &= \frac{1}{4E_\nu E_N v_{\rm rel}} \frac{d^3 k_\nu}{(2\pi)^3 2E'_\nu} \sum_{a=q,\bar{q}} \int_0^1 d\xi f_a^N(\xi, Q^2) \frac{E_N}{E_a} \int \frac{d^3 k_a}{(2\pi)^3 2E'_a} (2\pi)^4 \delta^{(4)}(\xi p_N + q - k_a) |\overline{\mathcal{M}}|^2 \\ &\simeq \frac{G_F^2}{2\pi} \frac{y}{(1 + Q^2/M_Z^2)^2} [p_\nu^\alpha k_\nu^\beta + p_\nu^\beta k_\nu^\alpha - g^{\alpha\beta}(k_\nu \cdot p_\nu) \pm i\varepsilon^{\alpha\beta\gamma\delta} p_{\nu,\gamma} k_{\nu,\delta}] \sum_{a=q,\bar{q}} F^a_{\alpha\beta} dx dy, \end{aligned} \tag{B9}$$

where $+\,(-)$ applies to neutrinos (antineutrinos); $G_F \simeq 1.167\,\times 10^{-5}$ GeV $^{-2}$ is the Fermi weak coupling constant; $|\overline{\mathcal{M}}|^2$ is the squared Feynman amplitude of the neutrino-quark elastic scattering averaged over the initial quark spins; $g^{\alpha\beta} = {\rm diag}(1,-1,-1,-1)$ is the Minkowski metric tensor; $\varepsilon^{\alpha\beta\gamma\delta}$ is the totally anti-symmetric tensor;

$f^N_{q(\bar{q})}$ is the Lorentz scalar PDF for the (anti)quark q ($\bar{q}$) in the nucleon N and we have neglected neutrino masses in comparison with the energies and other mass scales involved. The hadronic tensor $F^a_{\alpha\beta}$ related to (anti)quark $a = q(\bar{q})$ is defined as

$$F^a_{\alpha\beta} = \frac{f^N_a(x, Q^2)}{4Q^2} \sum_{\text{spins}} \langle a(xp_N)|J^a_\alpha|a(k_a)\rangle \times \langle a(k_a)|J^{a\dagger}_\beta|a(xp_N)\rangle, \tag{B10}$$

and the neutral quark current (multiplied by the numerator of the Z boson propagator and having factored out the electroweak coupling constant) as

$$J^q_\alpha = \left(g_{\alpha\beta} - \frac{q_\alpha q_\beta}{M_Z^2}\right) \bar{q}\gamma^\beta(g^q_V - g^q_A\gamma_5)q, \tag{B11}$$

where γ^α are the ordinary Dirac gamma matrices, $\gamma^5 = (i/4!)\varepsilon_{\alpha\beta\gamma\delta}\gamma^\alpha\gamma^\beta\gamma^\gamma\gamma^\delta$ is the fifth gamma matrix, and the couplings are given by $g^{u,\,c,\,t}_V = 1/2 - (4/3)s^2_W$, $g^{u,\,c,\,t}_A = 1/2$, $g^{d,\,s,\,b}_V = -1/2 + (2/3)s^2_{\rm W}$ and $g^{d,\,s,\,b}_A = -1/2$. We note that $F^a_{\alpha\beta}$ can only depend on the momenta p_N and q and thus decomposes into

$$\begin{aligned} F^a_{\alpha\beta} = &- g_{\alpha\beta}F^a_1 + \frac{p_{N\,\alpha}p_{N\,\beta}}{m_N^2}\frac{m_N}{\epsilon}F^a_2 - i\,\frac{\epsilon_{\alpha\beta\gamma\delta}p^\gamma_N q^\delta}{2m_N^2}\frac{m_N}{\epsilon}F^a_3 \\ &+ \frac{q^\alpha q^\beta}{m_N^2}F^a_4 + \frac{p^\alpha_N q^\beta + p^\beta_N q^\alpha}{2m_N^2}F^a_5 \\ &+ i\,\frac{p^\alpha_N q^\beta - p^\beta_N q^\alpha}{2m_N^2}F^a_6\,. \end{aligned} \tag{B12}$$

With the adopted decomposition of $F^a_{\alpha\beta}$, the quantities F^a_1, F^a_2, F^a_3, F^a_4, F^a_5 and F^a_6 are dimensionless. As can be checked, the third line proportional to F^a_6 gives vanishing contributions when contracted with the combination of leptonic momenta appearing in the second line of Eq. (B9). The same holds for the F^a_4 and F^a_5 contributions in the limit of vanishing neutrino masses. Thus, only the terms proportional to F^a_1, F^a_2 and F^a_3 are relevant in our calculation. We then get the following expressions for the F^a_1, F^a_2 and F^a_3 [32]:

$$F^{q(\bar{q})}_1 = \frac{1}{2}[(g^q_V)^2 + (g^q_A)^2] f^N_{q(\bar{q})}(x, Q^2), \tag{B13}$$

$$F^{q(\bar{q})}_2 = 2xF^{q(\bar{q})}_1 \tag{B14}$$

$$F^{q(\bar{q})}_3 = (-)2g^q_V g^q_A f^N_{q(\bar{q})}(x, Q^2). \tag{B15}$$

Plugging the above expressions in Eq. (B9), after contraction of the Lorentz indices, we arrive to [32, 33]:

$$\frac{d^2\sigma^{\rm DIS}_{\nu N}}{dxdy} \simeq \frac{G_F^2}{2\pi}\frac{Q^2}{[1 + Q^2/M_Z^2]^2}\left[yF^{ZN}_1(x, Q^2) + \frac{1}{xy}\left(1 - y - \frac{m_N^2}{Q^2}\right)F^{ZN}_2(x, Q^2) \pm \left(1 - \frac{y}{2}\right)F^{ZN}_3(x, Q^2)\right], \tag{B16}$$

where $+(-)$ for the scattering with (anti)neutrinos, while $F^{ZN}_1 = \sum_{a=q,\bar{q}} F^a_1$, $F^{ZN}_2 = \sum_{a=q,\bar{q}} F^a_2$ and $F^{ZN}_3 = \sum_{a=q,\bar{q}} F^a_3$. Note that, in the above formula, Q^2 should be given in terms of x, y and s as $Q^2 = (s - m_N^2 - m_\nu^2)xy$. It can be further simplified if we consider the sum of neutrinos and antineutrinos contributions, $\sigma^{\rm DIS}_{(\nu+\bar{\nu})N} = \sigma^{\rm DIS}_{\nu N} + \sigma^{\rm DIS}_{\bar{\nu}N}$:

$$\frac{d\sigma^{\rm DIS}_{(\nu+\bar{\nu})N}}{dxdy} \simeq \sum_{a=q,\bar{q}} \frac{G_F^2}{2\pi}\frac{Q^2[(g^a_V)^2 + (g^a_A)^2]f^N_a(x, Q^2)}{[1 + Q^2/M_Z^2]^2} \times \left(y - 2 + \frac{2}{y} - \frac{2m_N^2}{Q^2 y}\right). \tag{B17}$$

In the reference frame in which the neutrino is at rest, the variable x can be written as $x = (E_\nu - m_\nu)/(E_N y)$, from which we get $dx/dE_\nu = 1/(E_N y)$. Then, the DIS differential cross section that we need for the boosted neutrino flux calculation is given by:

$$\frac{d\sigma^{\rm DIS}_{(\nu+\bar{\nu})N}}{dE_\nu} = \frac{1}{E_N}\int_{y_{\rm min}}^{y_{\rm max}} \frac{dy}{y}\,\frac{d\sigma^{\rm DIS}_{(\nu+\bar{\nu})N}}{dxdy}, \tag{B18}$$

which leads to the expression given in Eq. (5) of the main text, where, to keep a shorter notation, we have written $d\sigma^{\rm DIS}_{\nu N}$ in place of $d\sigma^{\rm DIS}_{(\nu+\bar{\nu})N}$. As already specified, to evaluate numerically the quark PDFs, we made use of the Python package `parton` and the "CT10" PDF set [34]. The quark PDFs in the considered library are given for $x \geq x_{\rm min} = 10^{-8}$ and in the range $Q^2_{\rm min} = 1.69\,{\rm GeV} \leq Q^2 \leq Q^2_{\rm max} = 10^{10}\,{\rm GeV}$. This practically limits our ability to properly estimate the DIS cross section outside the energy range $Q^2_{\rm min}/(2m_\nu) \leq E_\nu - m_\nu \leq \min\{Q^2_{\rm max}/(2m_\nu), T^{\rm max}_\nu(T_N)\}$, where $T^{\rm max}_\nu(T_N)$ is the maximal kinetic energy the neutrino can have after an elastic scattering,

$$T_\nu^{\max}(T_N) = \frac{\left(T_N^2 + 2m_N T_N\right)}{T_N + (m_N + m_\nu)^2/(2m_\nu)}, \tag{B19}$$

and $T_N \equiv E_N - m_N$ the initial kinetic energy of the incoming nucleon. While we could rely on an interpolation between the elastic and inelastic regimes, we decided to remain conservative in our study setting to zero the DIS contribution outside the aforementioned energy range. In practice, this does not affect any of our predictions for the range of E_ν of interest for the UHE neutrino telescopes considered in our study. Finally, we note that the inelasticity parameter lies between $y_{\min} = (E_\nu - m_\nu)/E_N$ and $y_{\max} = \min\{1, (E_\nu - m_\nu)/(E_N x_{\min})\} = 1$.

Appendix C: Boosted Relic Neutrinos from Cosmic Rays: Revisited

We revisit the computation of the CR-induced boosted relic neutrino flux discussed in [13], implementing the full cross section with Q^2-dependence of the form factors, the DIS contribution and a mixed CR composition. Firstly, we note that the ES cross section in the low-energy limit $2m_\nu E_N \lesssim m_N^2$ [32] reads:

$$\frac{d\sigma_{\nu N}^{\rm ES}}{dE_\nu} \simeq \frac{G_F^2(s-m_N^2)^2}{16\pi s\, T_\nu^{\max}(T_N)}\left[(1-4s_{\rm W}^2)^2 + 3\,(G_{\rm A}(0))^2\right], \tag{C1}$$

with $T_\nu^{\max}(T_N)$ as given in Eq. (B19). The expression in Eq. (C1) resembles the expression reported in [13] in the same limit, apart from an overall $\mathcal{O}(1)$ factor. Our calculation of the cross section differs instead more, with respect to the one in [13], for $2m_\nu E_N \gtrsim m_N^2$.

We show in Fig. 4 the neutrino flux computed according to Eq. (2), with $m_\nu = 0.1\,\mathrm{eV}$, $D_{\rm eff} = 10\,\mathrm{kpc}$, $\bar\eta_\nu = 8\times 10^{13}$ roughly saturating the limit given in [13], and different benchmark cases described in what follows. Our choice of $D_{\rm eff}$ is motivated if the neutrino overdensity is localised on a scale of the order of the MW radius.

i) The red dashed line is obtained by taking the cross section as in (C1) after recasting the all-species CR flux as observed at Earth from [49] in the energy range $10^5\,\mathrm{GeV} \lesssim E_{\rm CR} \lesssim 200\,\mathrm{EeV}$ and assuming a pure proton composition from the lowest to the largest energies. With this procedure we obtain results that are comparable (but not overlapping) with those presented in [13].

ii) The dot-dashed purple line is obtained by considering the full Q^2-dependent cross section as a sum of the elastic and deep inelastic contributions, as discussed in the main text, while keeping the pure proton CR flux as in case i). We note a suppression compared to case i) starting from $E_\nu \sim \mathrm{EeV}$ due to the form factors $A_N(Q^2)$ and $C_N(Q^2)$ of the elastic cross section, as well as a kick at $E_\nu \sim 10\,\mathrm{EeV}$ because of the DIS.

iii) The thick yellow curve is obtained by considering the full cross section as in case ii) and a mixed composition for the CR flux according to the analysis presented in [14]. Concentrating on the extragalactic contribution only, we considered this flux in the energy range $10^8\,\mathrm{GeV} \lesssim E_{\rm CR} \lesssim 200\,\mathrm{EeV}$. For definiteness, we focused on the Scenario 1 described in [14], in which the proton composition gets suppressed earlier compared to heavier nuclei, thus implying an attenuation of the boosted relic neutrino flux.

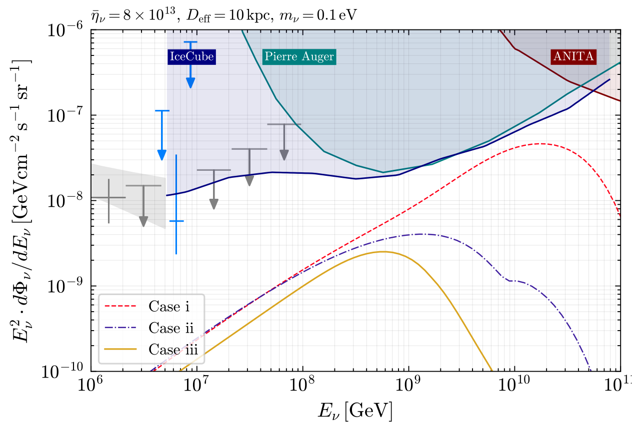

FIG. 4. Comparison between different procedures used to calculate the boosted all-flavour relic neutrino flux according to Eq. (2) of the main text, with $\bar\eta_\nu = 8\times10^{13}$, $D_{\rm eff} = 10\,\mathrm{kpc}$ and $m_\nu = 0.1\,\mathrm{eV}$. The dashed red line corresponds to case i) for which a low-energy limit of the elastic scattering cross section and a pure proton CR flux are considered; the dot-dashed purple line to case ii) with a full elastic plus inelastic cross section and a pure proton CR flux; the thick yellow line to case iii) with a full cross section and a mixed CR composition according to Scenario 1 of [14]. See the text for further details. The excluded regions and data points are as in Fig. 1.

We point out that the analogous flux in Fig. 1 is obtained as in case iii), but considering three neutrino species with masses that saturate the cosmological bound [59] – while that in Fig. 4 is for three degenerate neutrinos with reference mass $m_\nu = 0.1\,\mathrm{eV}$ – and starting the integration from $E_{\rm CR}^{\rm ankle}$ to remain conservative on the galactic-to-extragalactic transition.

We find that the implementation of the full momentum transfer dependence of the neutrino-nucleus cross section, the deep inelastic scattering contribution and a mixed CR composition, leads to a boosted relic neutrino flux suppressed significantly by an overall $\mathcal{O}(10)$ factor with respect to what reported in [13], and, correspondingly, the bounds on the local neutrino overdensity are weakened by the same amount.

Appendix D: Normalisation of the Cosmic Ray Flux Inside Galaxy Clusters

We discuss here the normalisation procedure that we followed for our estimate of the CR flux within galaxy clusters acting as CR-reservoirs. We rewrite here the flux of cosmic nucleus $\mathcal{N}$ as given in [30] and as used in our main analysis:

$$\frac{d\Phi_{\mathcal{N}}}{dE_{\mathcal{N}}} = K_{\mathcal{N}} \left(\frac{R_{\max}}{R}\right)^{\alpha} e^{-R/R_{\max}}. \tag{D1}$$

where the rigidity parameter R is defined as $R \equiv E_{\mathcal{N}}/(Z_{\mathcal{N}} q_e)$, q_e being the electric charge unit, with $R_{\max} = 2\times 10^{21}/26\,\mathrm{eV}$ [30] (for convenience, we absorb the electric charge q_e in the definition of R so that it is measured in eV rather than V). According to [30], at fixed R the chemical composition of $E^2_{\mathcal{N}} d\Phi_{\mathcal{N}}/dE_{\mathcal{N}}$ is (0.625, 0.252, 0.053, 0.009, 0.124) for (^{1}H, ^{4}He, CNO, ^{28}Si, ^{56}Fe) respectively (as reference for CNO we have considered ^{14}N only). Thus, at fixed R, we have

$$E^2_{\mathcal{N}} \frac{d\Phi_{\mathcal{N}}}{dE_{\mathcal{N}}} = Z^2_{\mathcal{N}} K_{\mathcal{N}} R^2 \left(\frac{R_{\max}}{R}\right)^{\alpha} e^{-R/R_{\max}}, \tag{D2}$$

so that the aforementioned proportions are reflected in the ratios of $Z^2_{\mathcal{N}} K_{\mathcal{N}}$. Therefore, $K_{\mathcal{N}} \equiv (C_{\mathrm{N}}/Z^2_{\mathrm{N}}) K_{\mathrm{H}}$, with $C_{\mathrm{He}} \simeq 0.4032$, $C_{\mathrm{N}} \simeq 0.0848$, $C_{\mathrm{Si}} \simeq 0.0144$ and $C_{\mathrm{Fe}} \simeq 0.1984$. The only parameter left to determine is K_H, which we fix by requiring that the luminosity emitted from the population of CR-reservoirs matches with the one observed at Earth, by, e.g., Pierre Auger above the ankle. More specifically, we impose

$$\sum_{\mathcal{N}} \int_{E_{\mathrm{CR}}^{\mathrm{ankle}}}^{E_{\mathrm{CR}}^{\max}} dE_{\mathcal{N}} E_{\mathcal{N}} \frac{d\Phi_{\mathcal{N}}}{dE_{\mathcal{N}}} = \int_{E_{\mathrm{CR}}^{\mathrm{ankle}}}^{E_{\mathrm{CR}}^{\max}} dE_{\mathrm{CR}} E_{\mathrm{CR}} \frac{d\Phi_{\mathrm{CR}}}{dE_{\mathrm{CR}}}, \tag{D3}$$

where the CR flux at Earth is taken from [93] to be $d\Phi_{\mathrm{CR}}/dE_{\mathrm{CR}} \simeq (d\Phi_{\mathrm{CR}}/dE_{\mathrm{CR}})_{\mathrm{ankle}} (E^{\mathrm{ankle}}_{\mathrm{CR}}/E_{\mathrm{CR}})^{2.5}$, with $(d\Phi/dE_{\mathrm{CR}})_{\mathrm{ankle}} \simeq 10^{-27}\,\mathrm{GeV^{-1}cm^{-2}s^{-1}sr^{-1}}$, within the range $E^{\mathrm{ankle}}_{\mathrm{CR}} = 5\,\mathrm{EeV} \leq E_{\mathrm{CR}} \leq E^{\max}_{\mathrm{CR}} = 200\,\mathrm{EeV}$. The CR flux observed at Pierre Auger and reported in [93] is actually more complicated than the single power-law considered above, including changes in the slopes at and above the ankle, mixed composition and a suppression at $\sim 50\,\mathrm{EeV}$. We have checked, however, that such additional features do not change appreciably the value of the integral in the right-hand-side of Eq. (D3), to which the shape at lower energies dominates. The integral on the left-hand-side can be computed analytically as follows:

$$\begin{aligned}
\sum_{\mathcal{N}} \int_{E_{\mathrm{CR}}^{\mathrm{ankle}}}^{E_{\mathrm{CR}}^{\max}} dE_{\mathcal{N}} E_{\mathcal{N}} \frac{d\Phi_{\mathcal{N}}}{dE_{\mathcal{N}}} &= K_{\mathrm{H}} \sum_{\mathcal{N}} \frac{C_{\mathcal{N}}}{Z^2_{\mathcal{N}}} \int_{E_{\mathrm{CR}}^{\mathrm{ankle}}}^{E_{\mathrm{CR}}^{\max}} dE_{\mathcal{N}}\, E_{\mathcal{N}} \left(\frac{E^{\max}_{\mathcal{N}}}{E_{\mathcal{N}}}\right)^{\alpha} e^{-E_{\mathcal{N}}/E^{\max}_{\mathcal{N}}} \\
&= K_{\mathrm{H}} \sum_{\mathcal{N}} C_{\mathcal{N}} R^2_{\max} \int_{E_{\mathrm{CR}}^{\mathrm{ankle}}/(Z_{\mathcal{N}} R_{\max})}^{E_{\mathrm{CR}}^{\max}/(Z_{\mathcal{N}} R_{\max})} dx\, x^{1-\alpha} e^{-x} \\
&= K_{\mathrm{H}} \sum_{\mathcal{N}} C_{\mathcal{N}} R^2_{\max} \left[\Gamma\left(2-\alpha, \frac{E^{\mathrm{ankle}}_{\mathrm{CR}}}{Z_{\mathcal{N}} R_{\max}}\right) - \Gamma\left(2-\alpha, \frac{E^{\max}_{\mathrm{CR}}}{Z_{\mathcal{N}} R_{\max}}\right)\right],
\end{aligned} \tag{D4}$$

where $\Gamma(a, z)$ is the upper incomplete Gamma function. For different values of the slope α, we find the normalisation factors listed in Table I.

Normalisation factors			
	$\alpha = 2$	$\alpha = 2.3$	$\alpha = 2.5$
K_{H}	1.94×10^{-30}	9.44×10^{-31}	5.20×10^{-31}
K_{He}	1.96×10^{-31}	9.52×10^{-32}	5.24×10^{-32}
K_{N}	3.36×10^{-33}	1.63×10^{-33}	8.99×10^{-34}
K_{Si}	1.43×10^{-34}	6.94×10^{-35}	3.82×10^{-35}
K_{Fe}	5.70×10^{-34}	2.77×10^{-34}	1.52×10^{-34}

TABLE I. Flux normalisation factors for each nuclear species considered and different benchmark values of α. All listed values are in units of $\mathrm{GeV^{-1}cm^{-2}s^{-1}sr^{-1}}$.

Appendix E: Results for Inverted Ordering

We report here the results of our analysis for a neutrino mass spectrum with IO, i.e. $m_3 < m_1 < m_2$, $\Delta m^2_{21} \equiv m^2_2 - m^2_1 = 7.42\times 10^{-5}\,\mathrm{eV}^2$ and $\Delta m^2_{23} \equiv m^2_3 - m^2_1 = 2.486\times 10^{-3}\,\mathrm{eV}^2$ [72], and sum of neutrino masses saturating the cosmological limit $\sum_i m_i = 0.145\,\mathrm{eV}$ [59]. In the hierarchical limit with $m_3 \ll m_1 \lesssim m_2$, there are two heavy and one light neutrino implying a flux that is larger by a factor ~ 2 with respect to the results in the NO case. Correspondingly, the limits and sensitivities on $\mathcal{B}\overline{\eta}_\nu$ are slightly improved compared to the case of NO. We note, however, that also the cluster mass limit becomes more stringent by an equal amount, for the same reason. In the degenerate limit $m_1 \simeq m_2 \simeq m_3$, the IO case is practically identical to the scenario with NO. The results for IO are summarised graphically in Fig. 5.

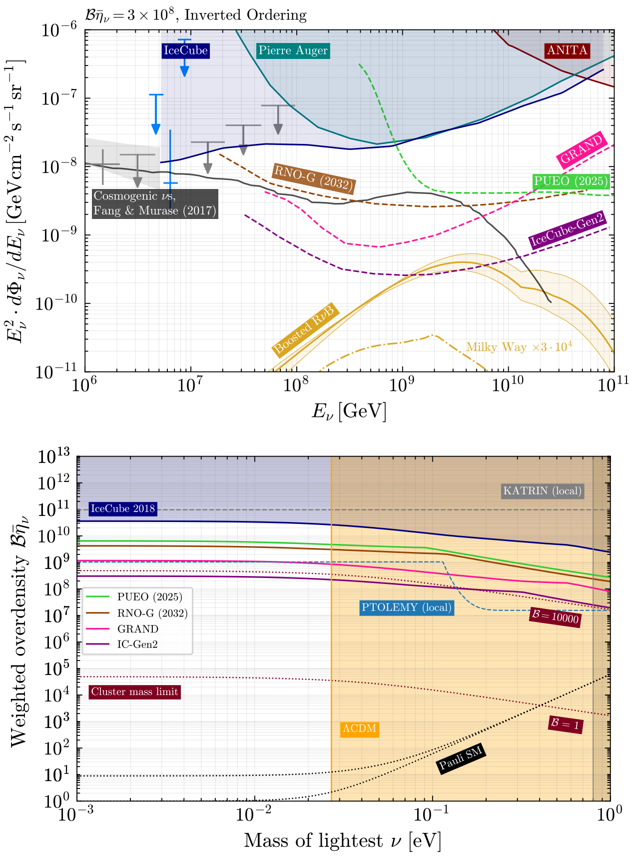

FIG. 5. Boosted all-flavour relic neutrino flux (upper panel) and corresponding limits and sensitivities on $\mathcal{B}\bar{\eta}_\nu$ (bottom panel) for a neutrino mass spectrum with IO. All legends are as in Figs. 1 and 2.

* andreagiovanni.demarchi@unibo.it
† alessandro.granelli@unibo.it
‡ jacopo.nava2@unibo.it
§ f.sala@unibo.it; FS is on leave from LPTHE, CNRS & Sorbonne Université, Paris, France.

[1] Julien Lesgourgues, Gianpiero Mangano, Gennaro Miele, and Sergio Pastor, *Neutrino Cosmology* (Cambridge University Press, 2013).

[2] N. Aghanim *et al.* (Planck), *Planck 2018 results. VI. Cosmological parameters,* Astronomy & Astrophysics **641**, A6 (2020), [Erratum: Astron.Astrophys. 652, C4 (2021)], arXiv:1807.06209 [astro-ph.CO].

[3] Gary Steigman, *Neutrinos And Big Bang Nucleosynthesis,* Advances in High Energy Physics **2012**, 268321 (2012), arXiv:1208.0032 [hep-ph].

[4] Martin Bauer and Jack D. Shergold, *Limits on the cosmic neutrino background,* Journal of Cosmology and Astroparticle Physics **01**, 003 (2023), arXiv:2207.12413 [hep-ph].

[5] E. Baracchini *et al.* (PTOLEMY), *PTOLEMY: A Proposal for Thermal Relic Detection of Massive Neutrinos and Directional Detection of MeV Dark Matter,* (2018), arXiv:1808.01892 [physics.ins-det].

[6] Yevheniia Cheipesh, Vadim Cheianov, and Alexey Boyarsky, *Navigating the pitfalls of relic neutrino detection,* Physical Review D **104**, 116004 (2021), arXiv:2101.10069 [hep-ph].

[7] A. Apponi *et al.* (PTOLEMY), *Heisenberg's uncertainty principle in the PTOLEMY project: A theory update,* Physical Review D **106**, 053002 (2022), arXiv:2203.11228 [hep-ph].

[8] M. Aker *et al.*, *New constraint on the local relic neutrino background overdensity with the first katrin data runs,* Physical Review Letters **129** (2022), 10.1103/physrevlett.129.011806.

[9] Yu-Dai Tsai, Joshua Eby, Jason Arakawa, Davide Farnocchia, and Marianna S. Safronova, *OSIRIS-REx constraints on local dark matter and cosmic neutrino profiles,* Journal of Cosmology and Astroparticle Physics **02**, 029 (2024), arXiv:2210.03749 [hep-ph].

[10] Andreas Ringwald and Yvonne Y. Y. Wong, *Gravitational clustering of relic neutrinos and implications for their detection,* Journal of Cosmology and Astroparticle Physics **12**, 005 (2004), arXiv:hep-ph/0408241.

[11] Tetsuya Hara and Humitaka Sato, *Scattering of the Cosmic Neutrinos by High Energy Cosmic Rays,* Progress of Theoretical Physics **64**, 1089–1092 (1980).

[12] Tetsuya Hara and Humitaka Sato, *Elastic and Inelastic Scattering of the Relic Neutrinos by High-energy Cosmic Rays,* Progress of Theoretical Physics **65**, 477 (1981).

[13] Mar Císcar-Monsalvatje, Gonzalo Herrera, and Ian M. Shoemaker, *Upper Limits on the Cosmic Neutrino Background from Cosmic Rays,* (2024), arXiv:2402.00985 [hep-ph].

[14] A. Abdul Halim *et al.* (Pierre Auger), *Constraining the sources of ultra-high-energy cosmic rays across and above the ankle with the spectrum and composition data measured at the Pierre Auger Observatory,* Journal of Cosmology and Astroparticle Physics **05**, 024 (2023), arXiv:2211.02857 [astro-ph.HE].

[15] R. U. Abbasi *et al.* (Telescope Array), *Mass composition of ultrahigh-energy cosmic rays with the Telescope Array Surface Detector data,* Physical Review D **99**, 022002 (2019), arXiv:1808.03680 [astro-ph.HE].

[16] Daniele Fargion, B. Mele, and A. Salis, *Ultrahigh-energy neutrino scattering onto relic light neutrinos in galactic halo as a possible source of highest energy extragalactic cosmic rays,* The Astrophysical Journal **517**, 725–733 (1999), arXiv:astro-ph/9710029.

[17] Thomas J. Weiler, *Cosmic ray neutrino annihilation on relic neutrinos revisited: A Mechanism for generating air showers above the Greisen-Zatsepin-Kuzmin cutoff,* Astroparticle Physics **11**, 303–316 (1999), arXiv:hep-ph/9710431.

[18] Jack Franklin, Ivan Martinez-Soler, Yuber F. Perez-Gonzalez, and Jessica Turner, *Constraints on the Cosmic Neutrino Background from NGC 1068,* (2024), arXiv:2404.02202 [hep-ph].

[19] Birgit Eberle, Andreas Ringwald, Liguo Song, and Thomas J. Weiler, *Relic neutrino absorption spectroscopy,* Physical Review D **70**, 023007 (2004), arXiv:hep-ph/0401203.

[20] M. G. Aartsen *et al.* (IceCube), *Differential limit on the extremely-high-energy cosmic neutrino flux in the presence of astrophysical background from nine years of IceCube data,* Physical Review D **98**, 062003 (2018),

arXiv:1807.01820 [astro-ph.HE].

[21] Alexander Aab *et al.* (Pierre Auger), *Probing the origin of ultra-high-energy cosmic rays with neutrinos in the EeV energy range using the Pierre Auger Observatory,* Journal of Cosmology and Astroparticle Physics **10**, 022 (2019), arXiv:1906.07422 [astro-ph.HE].

[22] Vedran Brdar, P. S. Bhupal Dev, Ryan Plestid, and Amarjit Soni, *A new probe of relic neutrino clustering using cosmogenic neutrinos,* Physics Letters B **833**, 137358 (2022), arXiv:2207.02860 [hep-ph].

[23] Kyrylo Bondarenko, Alexey Boyarsky, Josef Pradler, and Anastasia Sokolenko, *Best-case scenarios for neutrino capture experiments,* Journal of Cosmology and Astroparticle Physics **10**, 026 (2023), arXiv:2306.12366 [hep-ph].

[24] Alexei Yu. Smirnov and Xun-Jie Xu, *Neutrino bound states and bound systems,* Journal of High Energy Physics **08**, 170 (2022), arXiv:2201.00939 [hep-ph].

[25] H. J. Volk, F. A. Aharonian, and D. Breitschwerdt, *The nonthermal energy content and gamma-ray emission of starburst galaxies and clusters of galaxies,* Space Science Reviews **75**, 279–297 (1996).

[26] V. S. Berezinsky, P. Blasi, and V. S. Ptuskin, *Clusters of Galaxies as a Storage Room for Cosmic Rays,* The Astrophysical Journal **487**, 529–535 (1997), arXiv:astro-ph/9609048.

[27] Kohta Murase, Susumu Inoue, and Shigehiro Nagataki, *Cosmic Rays Above the Second Knee from Clusters of Galaxies and Associated High-Energy Neutrino Emission,* The Astrophysical Journal **689**, L105 (2008), arXiv:0805.0104 [astro-ph].

[28] K. Kotera, D. Allard, K. Murase, J. Aoi, Y. Dubois, T. Pierog, and S. Nagataki, *Propagation of ultrahigh energy nuclei in clusters of galaxies: resulting composition and secondary emissions,* The Astrophysical Journal **707**, 370–386 (2009), arXiv:0907.2433 [astro-ph.HE].

[29] Kohta Murase and John F. Beacom, *Galaxy Clusters as Reservoirs of Heavy Dark Matter and High-Energy Cosmic Rays: Constraints from Neutrino Observations,* Journal of Cosmology and Astroparticle Physics **02**, 028 (2013), arXiv:1209.0225 [astro-ph.HE].

[30] Ke Fang and Kohta Murase, *Linking High-Energy Cosmic Particles by Black Hole Jets Embedded in Large-Scale Structures,* Nature Physics **14**, 396–398 (2018), arXiv:1704.00015 [astro-ph.HE].

[31] Antonio Condorelli, Jonathan Biteau, and Remi Adam, *Impact of Galaxy Clusters on the Propagation of Ultrahigh-energy Cosmic Rays,* The Astrophysical Journal **957**, 80 (2023), arXiv:2309.04380 [astro-ph.HE].

[32] Carlo Giunti and Chung W. Kim, *Fundamentals of Neutrino Physics and Astrophysics* (Oxford University Press, Oxford, UK, 2007).

[33] J. A. Formaggio and G. P. Zeller, *From eV to EeV: Neutrino Cross Sections Across Energy Scales,* Reviews of Modern Physics **84**, 1307–1341 (2012), arXiv:1305.7513 [hep-ex].

[34] Hung-Liang Lai, Marco Guzzi, Joey Huston, Zhao Li, Pavel M. Nadolsky, Jon Pumplin, and C. P. Yuan, *New parton distributions for collider physics,* Physical Review D **82**, 074024 (2010), arXiv:1007.2241 [hep-ph].

[35] Daniel Z. Freedman, David N. Schramm, and David L. Tubbs, *The Weak Neutral Current and Its Effects in Stellar Collapse,* Annual Review of Nuclear and Particle Science **27**, 167–207 (1977).

[36] R. P. Feynman, M. Kislinger, and F. Ravndal, *Current matrix elements from a relativistic quark model,* Physical Review D **3**, 2706–2732 (1971).

[37] Dieter Rein and Lalit M. Sehgal, *Neutrino Excitation of Baryon Resonances and Single Pion Production,* Annals of Physics **133**, 79–153 (1981).

[38] Stefano Gabici, Carmelo Evoli, Daniele Gaggero, Paolo Lipari, Philipp Mertsch, Elena Orlando, Andrew Strong, and Andrea Vittino, *The origin of Galactic cosmic rays: challenges to the standard paradigm,* International Journal of Modern Physics D **28**, 1930022 (2019), arXiv:1903.11584 [astro-ph.HE].

[39] Julia Becker Tjus and Lukas Merten, *Closing in on the origin of Galactic cosmic rays using multimessenger information,* Physics Reports **872**, 1–98 (2020), arXiv:2002.00964 [astro-ph.HE].

[40] S. Thoudam, J. P. Rachen, A. van Vliet, A. Achterberg, S. Buitink, H. Falcke, and J. R. Hörandel, *Cosmic-ray energy spectrum and composition up to the ankle: the case for a second Galactic component,* Astronomy & Astrophysics **595**, A33 (2016), arXiv:1605.03111 [astro-ph.HE].

[41] Rafael Alves Batista *et al.*, *Open Questions in Cosmic-Ray Research at Ultrahigh Energies,* Frontiers in Astronomy and Space Sciences **6**, 23 (2019), arXiv:1903.06714 [astro-ph.HE].

[42] Alexander Aab *et al.* (Pierre Auger), *Cosmic-ray anisotropies in right ascension measured by the Pierre Auger Observatory,* The Astrophysical Journal **891**, 142 (2020), arXiv:2002.06172 [astro-ph.HE].

[43] A. Coleman *et al.*, *Ultra high energy cosmic rays The intersection of the Cosmic and Energy Frontiers,* Astroparticle Physics **149**, 102819 (2023), arXiv:2205.05845 [astro-ph.HE].

[44] R. U. Abbasi *et al.* (HiRes), *A Study of the composition of ultrahigh energy cosmic rays using the High Resolution Fly's Eye,* The Astrophysical Journal **622**, 910–926 (2005), arXiv:astro-ph/0407622.

[45] R. Aloisio, V. Berezinsky, and P. Blasi, *Ultra high energy cosmic rays: implications of Auger data for source spectra and chemical composition,* Journal of Cosmology and Astroparticle Physics **10**, 020 (2014), arXiv:1312.7459 [astro-ph.HE].

[46] R. U. Abbasi *et al.*, *Study of Ultra-High Energy Cosmic Ray composition using Telescope Array's Middle Drum detector and surface array in hybrid mode,* Astroparticle Physics **64**, 49–62 (2015), arXiv:1408.1726 [astro-ph.HE].

[47] R. U. Abbasi *et al.* (Telescope Array), *The Cosmic-Ray Composition between 2 PeV and 2 EeV Observed with the TALE Detector in Monocular Mode,* The Astrophysical Journal **909**, 178 (2021), arXiv:2012.10372 [astro-ph.HE].

[48] A. Abdul Halim *et al.* (Pierre Auger), *Constraining models for the origin of ultra-high-energy cosmic rays with a novel combined analysis of arrival directions, spectrum, and composition data measured at the Pierre Auger Observatory,* Journal of Cosmology and Astroparticle Physics **01**, 022 (2024), arXiv:2305.16693 [astro-ph.HE].

[49] Xing-Jian Lv, Xiao-Jun Bi, Kun Fang, Yi-Qing Guo, Hui-Hai He, Ling-Ling Ma, Peng-Fei Yin, Qiang Yuan, and Meng-Jie Zhao, *Precise measurement of the cosmic-ray spectrum and $\langle \ln A \rangle$ by LHAASO – connecting the Galactic to the extragalactic components,* (2024), arXiv:2403.11832 [astro-ph.HE].

[50] Gang Guo, Yue-Lin Sming Tsai, Meng-Ru Wu, and Qiang Yuan, *Elastic and Inelastic Scattering of Cosmic-Rays on Sub-GeV Dark Matter,* Physical Review D **102**, 103004 (2020), arXiv:2008.12137 [astro-ph.HE].

[51] Chen Xia, Yan-Hao Xu, and Yu-Feng Zhou, *Production and attenuation of cosmic-ray boosted dark matter,* Journal of Cosmology and Astroparticle Physics **02**, 028 (2022), arXiv:2111.05559 [hep-ph].

[52] R. Xu *et al.* (CDEX), *Constraints on sub-GeV dark matter boosted by cosmic rays from the CDEX-10 experiment at the China Jinping Underground Laboratory,* Physical Review D **106**, 052008 (2022), arXiv:2201.01704 [hep-ex].

[53] Tadeusz Wibig and Arnold W. Wolfendale, *Heavy Cosmic Ray Nuclei from Extragalactic Sources above 'The Ankle',* The Open Astronomy Journal **2**, 95–101 (2009), arXiv:0712.3403 [astro-ph].

[54] Andrew M. Taylor, Markus Ahlers, and Felix A. Aharonian, *The need for a local source of UHE CR nuclei,* Physical Review D **84**, 105007 (2011), arXiv:1107.2055 [astro-ph.HE].

[55] Silvia Mollerach and Esteban Roulet, *Ultrahigh energy cosmic rays from a nearby extragalactic source in the diffusive regime,* Physical Review D **99**, 103010 (2019), arXiv:1903.05722 [astro-ph.HE].

[56] Rodrigo Guedes Lang, Andrew M. Taylor, Markus Ahlers, and Vitor de Souza, *Revisiting the distance to the nearest ultrahigh energy cosmic ray source: Effects of extragalactic magnetic fields,* Physical Review D **102**, 063012 (2020), arXiv:2005.14275 [astro-ph.HE].

[57] Pavlo Plotko, Arjen van Vliet, Xavier Rodrigues, and Walter Winter, *Differences between the Pierre Auger Observatory and Telescope Array Spectra: Systematic Effects or Indication of a Local Source of Ultra-high-energy Cosmic Rays?* The Astrophysical Journal **953**, 129 (2023), arXiv:2208.12274 [astro-ph.HE].

[58] Gianfranco Brunetti and Thomas W. Jones, *Cosmic rays in galaxy clusters and their nonthermal emission,* International Journal of Modern Physics D **23**, 1430007 (2014), arXiv:1401.7519 [astro-ph.CO].

[59] A. G. Adame *et al.* (DESI), *DESI 2024 VI: Cosmological Constraints from the Measurements of Baryon Acoustic Oscillations,* (2024), arXiv:2404.03002 [astro-ph.CO].

[60] R. Abbasi *et al.* (IceCube), *Improved Characterization of the Astrophysical Muon–neutrino Flux with 9.5 Years of IceCube Data,* The Astrophysical Journal **928**, 50 (2022), arXiv:2111.10299 [astro-ph.HE].

[61] M. G. Aartsen *et al.* (IceCube), *Characteristics of the diffuse astrophysical electron and tau neutrino flux with six years of IceCube high energy cascade data,* Physical Review Letters **125**, 121104 (2020), arXiv:2001.09520 [astro-ph.HE].

[62] M. G. Aartsen *et al.* (IceCube), *Detection of a particle shower at the Glashow resonance with IceCube,* Nature **591**, 220–224 (2021), [Erratum: Nature 592, E11 (2021)], arXiv:2110.15051 [hep-ex].

[63] R. Abbasi *et al.* (IceCube), *The IceCube high-energy starting event sample: Description and flux characterization with 7.5 years of data,* Physical Review D **104**, 022002 (2021), arXiv:2011.03545 [astro-ph.HE].

[64] R. Abbasi *et al.*, *Characterization of the Astrophysical Diffuse Neutrino Flux using Starting Track Events in IceCube,* (2024), arXiv:2402.18026 [astro-ph.HE].

[65] *Differential Sensitivity of the KM3NeT/ARCA detector to a diffuse neutrino flux and to point-like source emission: exploring the case of the Starburst Galaxies,* (2024), arXiv:2402.09088 [astro-ph.HE].

[66] P. W. Gorham *et al.* (ANITA), *Constraints on the ultrahigh-energy cosmic neutrino flux from the fourth flight of ANITA,* Physical Review D **99**, 122001 (2019), arXiv:1902.04005 [astro-ph.HE].

[67] Q. Abarr *et al.* (PUEO), *The Payload for Ultrahigh Energy Observations (PUEO): a white paper,* Journal of Instrumentation **16**, P08035 (2021), arXiv:2010.02892 [astro-ph.IM].

[68] Marco Stein Muzio *et al.* (RNO-G), *Multimessenger Potential of the Radio Neutrino Observatory in Greenland,* Proceedings of Science **ICRC2023**, 1485 (2023), arXiv:2308.07224 [astro-ph.HE].

[69] Rasha Abbasi *et al.* (IceCube-Gen2), *Sensitivity studies for the IceCube-Gen2 radio array,* Proceedings of Science **ICRC2021**, 1183 (2021), arXiv:2107.08910 [astro-ph.HE].

[70] Jaime Álvarez-Muñiz *et al.* (GRAND), *The Giant Radio Array for Neutrino Detection (GRAND): Science and Design,* Science China Physics, Mechanics & Astronomy **63**, 219501 (2020), arXiv:1810.09994 [astro-ph.HE].

[71] *NuFit 5.2,* http://www.nu-fit.org.

[72] Ivan Esteban, M. C. Gonzalez-Garcia, Michele Maltoni, Thomas Schwetz, and Albert Zhou, *The fate of hints: updated global analysis of three-flavor neutrino oscillations,* Journal of High Energy Physics **09**, 178 (2020), arXiv:2007.14792 [hep-ph].

[73] Julio F. Navarro, Carlos S. Frenk, and Simon D. M. White, *A universal density profile from hierarchical clustering,* The Astrophysical Journal **490**, 493–508 (1997).

[74] R. L. Workman and Others (Particle Data Group), *Review of Particle Physics,* Progress of Theoretical and Experimental Physics **2022**, 083C01 (2022).

[75] M. Aker *et al.* (KATRIN), *Direct neutrino-mass measurement with sub-electronvolt sensitivity,* Nature Physics **18**, 160–166 (2022), arXiv:2105.08533 [hep-ex].

[76] Andrea Palladino and Francesco Vissani, *The natural parameterization of cosmic neutrino oscillations,* The European Physical Journal C **75**, 433 (2015), arXiv:1504.05238 [hep-ph].

[77] Mauricio Bustamante, John F. Beacom, and Walter Winter, *Theoretically palatable flavor combinations of astrophysical neutrinos,* Physical Review Letters **115**, 161302 (2015), arXiv:1506.02645 [astro-ph.HE].

[78] B. Pontecorvo, *Mesonium and anti-mesonium,* Journal of Experimental and Theoretical Physics **6**, 429 (1957).

[79] B. Pontecorvo, *Inverse beta processes and nonconservation of lepton charge,* Journal of Experimental and Theoretical Physics **34**, 247 (1957).

[80] Ziro Maki, Masami Nakagawa, and Shoichi Sakata, *Remarks on the unified model of elementary particles,* Progress of Theoretical Physics **28**, 870–880 (1962).

[81] M. G. Aartsen *et al.* (IceCube), *Flavor Ratio of Astrophysical Neutrinos above 35 TeV in IceCube,* Physical Review Letters **114**, 171102 (2015), arXiv:1502.03376 [astro-ph.HE].

[82] Andrea Palladino, *The flavor composition of astrophysical neutrinos after 8 years of IceCube: an indication of neutron decay scenario?* The European Physical Journal C **79**, 500 (2019), arXiv:1902.08630 [astro-ph.HE].

[83] M. G. Aartsen *et al.* (IceCube-Gen2), *IceCube-Gen2: the window to the extreme Universe,* Journal of Physics

G: Nuclear and Particle Physics **48**, 060501 (2021), arXiv:2008.04323 [astro-ph.HE].

[84] Alan Coleman, Oscar Ericsson, Mauricio Bustamante, and Christian Glaser, *The flavor composition of ultra-high-energy cosmic neutrinos: measurement forecasts for in-ice radio-based EeV neutrino telescopes,* (2024), arXiv:2402.02432 [astro-ph.HE].

[85] F. J. Ernst, R. G. Sachs, and K. C. Wali, *Electromagnetic form factors of the nucleon,* Physical Review **119**, 1105–1114 (1960).

[86] L. N. Hand, D. G. Miller, and Richard Wilson, *Electric and magnetic form factors of the nucleon,* Reviews of Modern Physics **35**, 335–349 (1963).

[87] C. F. Perdrisat, V. Punjabi, and M. Vanderhaeghen, *Nucleon Electromagnetic Form Factors,* Progress in Particle and Nuclear Physics **59**, 694–764 (2007), arXiv:hep-ph/0612014.

[88] J. M. Alarcón, D. W. Higinbotham, and C. Weiss, *Precise determination of the proton magnetic radius from electron scattering data,* Physical Review C **102**, 035203 (2020), arXiv:2002.05167 [hep-ph].

[89] Haiyan Gao and Marc Vanderhaeghen, *The proton charge radius,* Reviews of Modern Physics **94**, 015002 (2022), arXiv:2105.00571 [hep-ph].

[90] Constantia Alexandrou, Simone Bacchio, Martha Constantinou, Jacob Finkenrath, Roberto Frezzotti, Bartosz Kostrzewa, Giannis Koutsou, Gregoris Spanoudes, and Carsten Urbach (Extended Twisted Mass), *Nucleon axial and pseudoscalar form factors using twisted-mass fermion ensembles at the physical point,* Physical Review D **109**, 034503 (2024), arXiv:2309.05774 [hep-lat].

[91] Joshua Ellis, *TikZ-Feynman: Feynman diagrams with TikZ,* Comput. Phys. Commun. **210**, 103–123 (2017), arXiv:1601.05437 [hep-ph].

[92] Michael E. Peskin and Daniel V. Schroeder, *An Introduction to quantum field theory* (Addison-Wesley, Reading, USA, 1995).

[93] Alexander Aab *et al.* (Pierre Auger), *Features of the Energy Spectrum of Cosmic Rays above 2.5×10^{18} eV Using the Pierre Auger Observatory,* Physical Review Letters **125**, 121106 (2020), arXiv:2008.06488 [astro-ph.HE].